Mn3O4@ZnO Hybrid Material: An excellent photocatalyst for the degradation of synthetic dyes including methylene blue, methyl orange and malachite green

Benazir Shaikh, Muhammad Ali Bhatti, Aqeel Ahmed Shah, Aneela Tahira, Abdul Karim Shah, Azam Usto, Umair Aftab, Sarah Bukhari, Sultan Alshehri, Syed Nizam Uddin Shah Bukhari, et al.

Mn_3O_4@ZnO hybrid material: An excellent photocatalyst for the degradation of synthetic dyes including methylene blue, methyl orange and malachite green

Benazir Shaikh[a], Muhammad Ali Bhatti[a], Aqeel Ahmed Shah[b], Aneela Tahira[c*], Abdul Karim Shah[d], Azam Usto[d], Umair Aftab[e], Sarah I Bukhari[f], Sultan Alshehri[f], Syed Nizam Uddin Shah Bukhari[g,h], Matteo Tonezzer[i], Brigitte Vigolo[j], Zafar Hussain Ibupoto[c]*

[a]Institute of Environmental Sciences, University of Sindh Jamshoro, 76080, Sindh Pakistan
[b] Wet Chemistry Laboratory, Department of Metallurgical Engineering, NED University of Engineering and Technology, Karachi, Sindh Pakistan
[c]Dr. M.A Kazi Institute of Chemistry University of Sindh Jamshoro, 76080, Sindh Pakistan
[d]Department of Chemical Engineering, Dawood University of Engineering and Technology, Karachi, Pakistan
[e] Department of Metallurgy and Materials Engineering, Mehran University of Engineering and Technology, 7680 Jamshoro, Sindh Pakistan
[f] Department of Pharmaceutics, College of Pharmacy, King Saud University, Riyadh 11451, Saudi Arabia
[g] State Key Laboratory of Organic-Inorganic Composites, Beijing Key Laboratory of Electrochemical Process and Technology for Materials, school of Material Science, Beijing University of Chemical Technology, Beijing, 100029 China
[h] Department of Basic Science and Humanities, Dawood University of Engineering and Technology, Karachi, Sindh, 74800 Pakistan
[i]IMEM-CNR, Sede di Trento-FBK, Via alla Cascata 56/C, 38123 Trento, Italy
[j]Université de Lorraine, CNRS, IJL, F-54000 Nancy, France

* Correspondence: **authors:** Zafar Hussain Ibupoto & Aneela Tahira
Email: zaffar.ibhupoto@usindh.edu.pk; aneelatahira80@gmail.com

Abstract: Environmental pollution caused by organic dyes threatens life on land and in water. Therefore, immediate planning and action is needed to eliminate environmental pollution using new technologies, but sadly to this date it has remained a challenging task. In this study, we synthesized hybrid systems based on zinc oxide/manganese oxide (Mn_3O_4@ZnO) using sol gel and hydrothermal methods. The hybrid materials exhibited hierarchical morphologies and structures characterized by the hexagonal phase of ZnO and the tetragonal phase of Mn_3O_4. The hybrid materials were tested for degradation of methylene blue (MB), methyl orange (MO), and malachite green (MG) under ultraviolet (UV) light illumination. in the aim of this work was to observe the effect that various amounts of Mn_3O_4 in the hybrid material have on the degradation of MB, MO and MG. The ZnO photocatalyst showed better performance with an increasing amount of Mn_3O_4 and the degradation efficiency for the hybrid material containing the maximum amount of Mn_3O_4 was found to be 94.59 %, 89.99 % and 97.40 % for MB, MO and MG, respectively. The improvement in the performance of hybrid materials can be attributed to high charge separation rate of electron-hole pairs, co-catalytic role, large amount of catalytic sites and the synergy for the production of high quantities of oxidizing radicals. The performance obtained from the various Mn_3O_4@ZnO hybrid materials suggest that Mn_3O_4 can be considered an effective co-catalyst for a wide range of photocatalytic materials such as titanium dioxide, tin oxide and carbon-based materials in developing practical hybrid photocatalysts for the degradation of dyes and wastewater treatment.

Keywords: ZnO; Mn_3O_4; Mn_3O_4@ZnO; hybrid material; photocatalytic applications

1. Introduction

Environmental pollution caused by the extensive use of synthetic dyes, pigments and other coloring products in various industries such as food, beverages, cosmetics, pharmaceuticals, clothes and paper [1]. These chemical compounds are characterized by a complicated structure, high stability and are highly toxic to living things. In addition, the presence of dyes in wastewater prevents the transmission of sunlight deep into the water, damaging aquatic life. At the same time, these dyes are harmful to humans by causing breathing problems, vomiting, cancer, allergies, and skin problems [2]. Approximately 700000 tons of dyes are produced worldwide each year, and many end up in the wastewater of the textile industries, contaminating water resources and aquatic life as they are very toxic to our environment [3, 4]. Among them, malachite green (MG) and methylene blue (MB) are cationic, while methyl orange (MO) is anionic in nature [5,6].

Currently, the removal and degradation of dyes from wastewater before discharging it from reservoirs is seriously considered, but it still seems like a very difficult challenge. There are numerous methods for wastewater treatment

including coagulation, electro precipitation, adsorption, evaporation, reverse osmosis, flocculation, oxidation and photodegradation under the illumination of ultraviolet and solar light [7, 8]. Many of these methods are complicated, expensive, and have poor dye removal performance, while photodegradation is a simple, low cost and efficient method of removing organic dyes from wastewater [9, 10]. The challenge in photocatalytic degradation is the unavailability of highly efficient yet inexpensive photocatalysts. For this purpose, several photocatalytic materials have been prepared and tested for the degradation of dyes, such as ZnO [11], $BiFeO_3$ [12], TiO_2 [10], Cu_2O/LDH [13], Chitosan ZnO composite [14], $CuCl_2$ + STS, chitosan-g-Poly (acrylamide)/ZnS [15], Chitosan/$LaFe_{0.8}Cu_{0.2}O_3$ and xylan/$LaFe_{0.8}Cu_{0.2}O_3$ [16].

Among these well-known semiconducting materials, ZnO is highly studied for various applications including photocatalysis, chemical sensing and photovoltaics due to its tunable band gap (3.37 eV) and high exciton binding energy (60 meV) [17,18,19,20]. The role of the nanostructured morphology of ZnO is intensively investigated, therefore different morphologies of ZnO are reported such as 3D hollow spheres, 1D nanorods and nanowires and 2D nanobelts and nanosheets [21,22,23,24]. The advantageous features of these morphologies such as swift mass transfer, hierarchical structures and high surface area have been utilized for different applications such as chemical sensors, lithium-ion batteries and photocatalysis [25,26] .However, for the growing concern for the environment requires the development of nanostructured materials without or with minimum use of harmful chemicals 27,28,29]. Therefore, it is essential of synthesize ZnO-based nanostructures with maximum photocatalytic efficacy in an eco-friendly manner. Manganic oxide (Mn_3O_4) is an emerging p-type semiconductor with significant photocatalytic properties [30, 31]. Previously, Mn_3O_4 has demonstrated very good in photocatalytic applications , especially in combination with other metal oxides[32,33,34,35,36,37,38,39,40]. ZnO has many positive aspects such as high quantum efficiency, rich defect chemistry and cost effectiveness, and is therefore widely used for photocatalysis [39, 40]. The synthesis of hierarchical nanostructures of hybrid material based on Mn_3O_4@ZnO with improved electron-hole pairs separation and high density of electrons in the conduction band of ZnO could lead to more efficient photodegradation of MB, MO and MG under ultraviolet light illumination. A hybrid system based on Mn_3O_4@ZnO for efficient degradation of MB, MO and MG has not yet been reported in the exiting scientific literature.

In this study, we prepared the Mn_3O_4@ZnO hybrid material using the sol gel method followed by the hydrothermal method. Morphology, crystalline structure and chemical composition were studied with different analytical techniques such as SEM, XRD and EDS. The optimized Mn_3O_4@ZnO hybrid system revealed excellent photoactivity in the degradation of MB, MO and MG under UV light illumination.

2. Materials and methods

2.1. Materials used

Potassium permanganate ($KMnO_4$), glycerol, zinc acetate dihydrate, 33% aqueous ammonia, ethanol, sodium hydroxide, hydrochloric acid, methyl orange, methylene blue, and malachite green were purchased from Sigma Aldrich, Karachi Pakistan. The chemicals used were of a high analytical grade and were used without pretreatment. All desired concentrations of each reagent were prepared in deionized water.

2.2. Synthesis of Z Mn_3O_4@ZnO hybrid materials using sol gel and hydrothermal methods

The synthesis of the nanostructured hybrid material was carried out in two steps. The Mn_3O_4 nanostructures were prepared using the sol gel method and the typical synthesis process is described below. The Mn_3O_4 material was reproduced according to the work reported in[41]. Precursor solutions of 0.4 M glycerol and 0.3M potassium permanganate were prepared. Then the glycerol and potassium permanganate solutions were mixed in a ratio of 1:2 by volume, stirred for 2 h and finally kept for 24 h without disturbance to obtain the desired gel at room temperature. Afterwards, the gel was heated at 80 °C for 30 min and the product precipitates were obtained, and centrifugation was used to collect the fine brown colored Mn_3O_4 powder. Meanwhile the precursor ZnO was prepared by mixing 0.1 M of zinc acetate dihydrate and 5 mL of 33% aqueous ammonia solution in 100 mL of deionized water. Different amounts of Mn_3O_4 were deposited on the ZnO by the hydrothermal method: 0.3, 0.5, 0.75 and 1.0 grams of precipitated Mn_3O_4 were dissolved in four beakers containing 200 mL of a precursor solution of ZnO, in in order to develop hybrid Mn_3O_4@ZnO systems. The materials were labeled as sample 1, sample 2, sample 3, and sample 4, respectively. A fifth beaker was only containing the ZnO precursor solution and the pristine ZnO sample was used as a comparison. After being mixed, the solutions were covered very tightly with aluminum foil and left for hydrothermal reaction in a preheated electric oven for 5 h at 95 °C. After completion of the reaction, the beakers were cooled down to room temperature and the product was collected on filter paper and washed several times with ethanol followed by deionized water. In the end, the product was dried at 60 °C overnight.

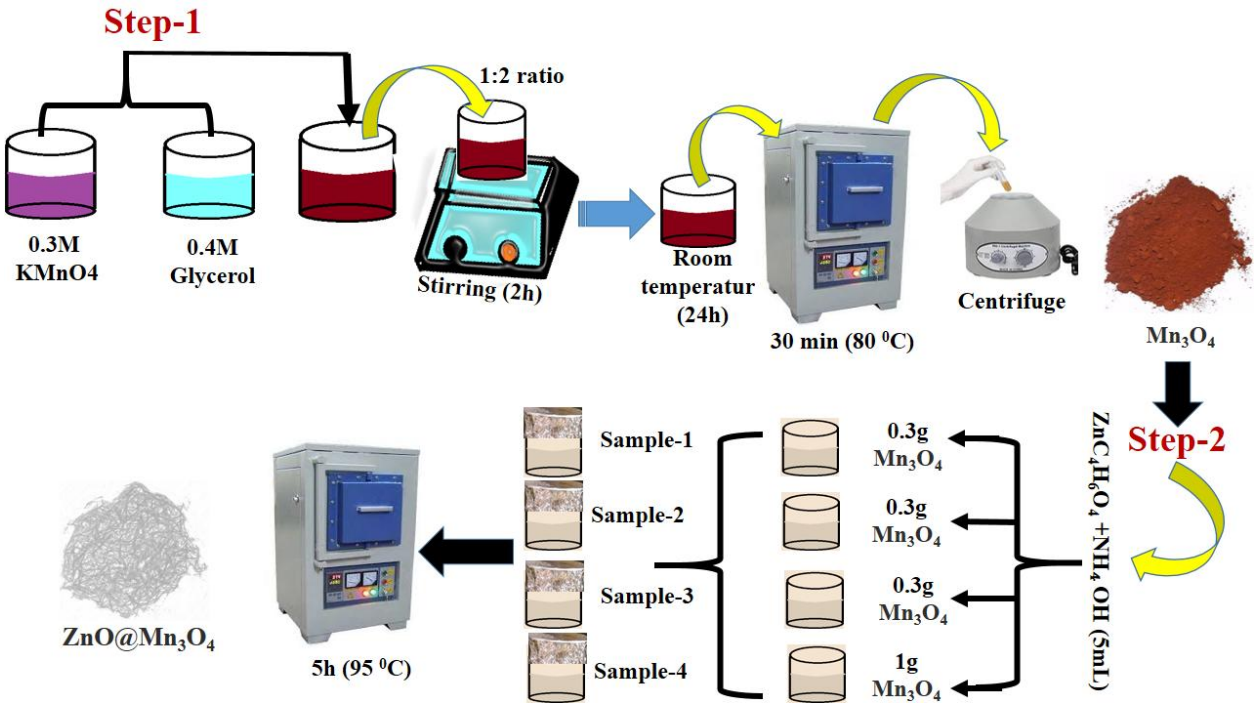

Scheme 1. Stepwise synthesis of Mn_3O_4@ZnO hybrid materials using sol gel and hydrothermal methods.

2.3. Characterization of morphology, crystalline structure, and chemical composition of the materials

Scanning electron microscopy was used at 10 kV to evaluate the morphology of the prepared nanostructured materials. Powder X-ray diffraction was employed at 45 mA and 45 kV to identify the crystal structure and phase of the nanostructured materials. Energy dispersive spectroscopy was used to quantify the elemental composition of each synthesized material. UV-visible spectrophotometry was employed to record absorption spectra during dye degradation under UV light illumination. The UV light source consisted of six UV tubes with a wavelength of 365 nm.

In this study, we studied the performance of hybrid materials for the degradation of various dyes (methylene blue, methyl orange, and malachite green) using 5 mg of each catalyst nanomaterial and a fixed concentration for each dye (1.87×10^{-5} M MB, 2.44×10^{-5} M MO, and 5.48×10^{-5} M MG). Before irradiation with UV light, the dye solution was stirred for 30 min in order to optimize its homogeneity.

The % degradation efficiency of each dye was estimated from the following equation:

$$\text{dye removal \%} = \frac{Co-Ct}{Co}\times 100 \qquad (1)$$

where C_o and C_t are the concentrations of each dye before and after degradation, respectively.

3. Results and discussion

3.1. Characterization of morphology, crystalline structure, and chemical composition of the Mn_3O_4@ZnO hybrid materials

Fig. 1 shows the XRD patterns of the different samples with increasing amounts of Mn_3O_4. The pattern obtained from the pure ZnO sample shows all the characteristic peaks of the material, as can be seen from the comparison with the black reference at the bottom of the figure (JCPDS sheet: 01-079-0207). In detail, the peaks present at 31.66°, 34.29°, 36.23°, 47.48°, 56.60°, 62.77° and 67.85° can be attributed to the planes (100), (002), (101), (102), (110), (103) and (200) of the hexagonal structure of the ZnO wurtzite. The patterns obtained from the hybrid samples also show the peaks from ZnO, but their relative intensity decreases, while that of the peaks from the tetragonal phase of Mn_3O_4 increases (JCPDS sheet: 00-003-1041, in blue at the bottom of the figure). The XRD patterns shown in Fig. 1 demonstrate that the Mn_3O_4@ZnO hybrid was successfully prepared. The nanomaterial is composed of ZnO and Mn_3O_4, while no amorphous phases or impurities were observed. As seen in Fig. 1b, the addition of Mn_3O_4 has the effect of slightly shifting the position of peak 220 to higher angles, suggesting an imperfection in the structure of the nanocrystals.

The SEM images in Fig. 2 show the morphology of pure ZnO and of the Mn_3O_4@ZnO hybrids. Pure ZnO appears to be made up of flower-like structures composed of nanorods with a diameter of 200-500 nm (Fig. 2a). Conversely, the morphology of hybrid nanomaterials appears to change towards very thin sheets as the Mn_3O_4 content increases (Fig. 2b-e). The morphology of all the samples is very homogeneous to indicate a good mixing of ZnO and Mn_3O_4 during the

hydrothermal process. The elemental composition of the materials was studied by energy dispersion X-ray spectroscopy, and the spectra are shown in Figure 3. The spectrum of pure ZnO (Fig. 3a) shows only peaks relative to Zn and O, while the other samples show the presence of Zn, O and Mn (Fig. 3b-e). The atomic percentage of manganese increases from Sample 1 to Sample 4, as expected.

3.2. Photocatalytic degradation of MB, MO and MG onto different Mn_3O_4@ZnO hybrid systems

The photodegradation of MB, MO and MG in aqueous solution using pure ZnO and the different hybrid systems ZnO @ Mn_3O_4 was studied under UV light illumination.

a. Methylene blue

Figure 4 shows the absorption spectra of pure ZnO during MB degradation over time under UV light illumination. A solution of MB with a concentration of 1.87×10^{-5} M was used to which 5 mg of catalyst was added. The spectra show a typical absorption peak around 663 nm which slowly decreases over time, indicating that the degradation rate is limited and therefore takes a long time. This suggests that pure ZnO exhibits a low density of catalytic sites and a high rate of recombination of the electron-hole pair, and therefore the release of oxidizing agents under illumination is limited, thus leading to poor MB degradation performance. The degradation kinetics was also studied as shown in Figure 4b,c. The reaction rate of MB degradation was evaluated by monitoring the change in concentration C_t over time from the initial concentration C_o, as shown in Figure 4b. Clearly the photoactivity of pure ZnO is highly correlated to the illumination time. The rate constant (K) of the photodegradation process was also calculated using the first order reaction equation [43]:

$$K_t = Ln(C_0/C_t)$$

The reaction kinetics was also studied as $\ln(C_0/C_t)$ over the illumination time, and is shown in Figure 4c. The rate constant for MB degradation using pure ZnO was found to be 1.14×10^{-3}min, confirming that the reaction follows first order kinetics. The degradation efficiency of pure ZnO photocatalyst was found to be 69.60 % as shown in Figure 4d, indicating that the performance of pure ZnO is not sufficient and the photocatalytic properties must be improved in order to exploit the true potential of this material for practical applications.

The degradation of MB was also performed using the various samples in order to verify how the degradation rate is affected by the composition of the hybrid material, and the spectra are shown in Figure 5a-d. The four panels show that all samples work better as photocatalysts than pure ZnO. Furthermore, comparing the decrease of the absorption spectrum over time in the four panels it is clear that a higher amount of Mn_3O_4 in the hybrid material greatly improves the degradation of MB. This trend could be attributed to the role of Mn_3O_4 in separating the charges of the electron-hole pairs, resulting in the production of a high amount of oxidizing radicals that play an important role in driving the degradation of MB in aqueous solution. The reaction kinetics was investigated for the hybrid samples of Mn_3O_4@ZnO and the ratio between the concentration of MB at a certain time C_t to the initial concentration C_o is shown in Figure 6a. The degradation of MB on hybrid materials clearly dependes on the illumination time. The reaction kinetics in terms of order of reaction was studied by calculating $Ln(C_0/C_t)$ over time (Fig. 6b) and it was found that the rate constant was characterized by first order kinetics. The rate constant (K) values for samples 1, 2, 3 and 4 were estimated to be 3.33×10^{-3}min, 4.19×10^{-3}min, 7.33×10^{-3}min, and 8.51×10^{-3}min, respectively. These values of rate constant suggest that a higher amount of Mn_3O_4 in the hybrid material significantly improves the degradation kinetics of MB in aqueous solution under UV light illumination. The degradation efficiency was calculated from the absorbance spectra and plotted over time for each hybrid system in Figure 6d. The hybrid Mn_3O_4@ZnO system with the highest amount of Mn_3O_4 (sample 4) was the most efficient with a degradation efficiency of 94.59 % for MB. The degradation efficiency of the other hybrid samples 1, 2, and 3 was 82.07 %, 85.28 %, and 92.91 %, respectively.

b. Methyl orange

The photodegradation of methyl orange was investigated with a solution with a concentration of 2.44×10^{-5}M and 5 mg of photocatalyst under UV light illumination. In the case of pure ZnO (Fig. 7), the degradation was found to be very poor due to the stable nature of the material, limited number of active sites and the rapid rate of charge recombination. The absorption trend is very slow, which means that the reaction rate is associated with a high activation energy using pure ZnO as photocatalyst. Poor performance in the degradation of MO by pure ZnO indicates that it is not a suitable material for this application. The reaction kinetics was studied by evaluationg the concentration of MO over time Ct with respect to the initial concentration Co, and the plot in Fig. 7b shows that the degradation is linear with respect to the irradiation time with UV light. The reaction kinetics with respect to UV light irradiation time turned out to be of the first order and the rate constant was calculated to be 6.44×10^{-4} min^{-1}, as shown in Figure 7c. The degradation efficiency

for MO was calculated from the absorption spectra of MO over a time of 320 minutes, and the calculated value was 73.56 %, as shown in Figure 7d. The four different hybrid samples were tested for the degradation of MO using a solution with a concentration of 2.44×10^{-5}M and 5 mg of each hybrid catalyst. The degradation experiments lasted 240 min and an adsorption spectrum was acquired every 30 minutes, as shown in Figure 8. Comparing the plots in Fig. 8 with that in Fig. 7a, it is clear, albeit qualitatively, that the degradation is in all cases better than that of pure ZnO. This indicates that the presence of Mn_3O_4 in the ZnO@Mn_3O_4 hybrid material increases the density of active sites and decreases the charge recombination rate of electron-hole pairs. In fact, the degradation of MO increases as the quantity of Mn_3O_4 present in the hybrid photocatalyst increases, i.e. from sample 1 to sample 4. The degradation kinetics of MO was also studied by evaluating how the MO concentration over time C_t varies with respect to the initial concentration C_o (Fig. 9a). The Ln of as the ratio is instead shown in Figure 9b. As can be seen in both panels, the degradation rate strongly depends on the irradiation time with UV light. The reaction kinetics of the four hybrid photocatalysts are of the first order and the rate constant values obtained for samples 1, 2, 3 and 4 are respectively 2.32×10^{-3}min, 2.50×10^{-3}min, 2.74×10^{-3}min and 4.58×10^{-3}min. The percent degradation efficiency of samples 1, 2, 3 and 4 was calculated and found to be 82.78 %, 83.38 %, 85.12 %, and 89.99 %, respectively, as shown in Figure 9c. It is therefore clear that the degradation efficiency for MO increases as the quantity of Mn_3O_4 in the hybrid material increases.

c. Malachite green

Considering the high toxicity of MG to aquatic life and human health, pure ZnO and Mn_3O_4@ZnO hybrid materials were tested for the degradation of MG under UV light illumination. In the experiments, a solution of MG with a concentration of 5.48×10^{-5}M and 5 mg of catalyst were used. Figure 10 shows the maximum absorption peak of MG at 617 nm and its evolution over time in the presence of pure ZnO. The adsorption peak decreases confirming the catalytic activity, however the degradation process is relatively slow and the efficiency is not very high due to the wide band gap of pure ZnO, its fast charge recombination rate and its low density of catalytic sites. The reaction rate of MG with pure ZnO was studied quantitatively by plotting the ratio between the concentration over time Ct and the initial concentration C_o, and it is clear that the degradation of MG strongly depends on the time of irradiation with UV light (Figure 10b). Furthermore, plotting LnC_o/C_t as in Figure 10c, it can be seen that the reaction kinetics are of the first order. The percent degradation efficiency was calculated obtaining a value of 85.37 %, as shown in Figure 10d. The performance of pure ZnO was therefore unsatisfactory, demonstrating that the material must be functionalized to efficiently degradade MG under UV light illumination.

In this sense, the hybrid materials Mn_3O_4@ZnO were also tested, whose absorption spectra over time are shown in Figure 11. All materials functionalized with Mn_3O_4 proved to be highly efficient for the degradation of MG, as can be seen from the strong decrease of the absorption peak at 617 nm. Note that the degradation experiment in this case only lasted 70 minutes. Comparing the four panels (a-d) it can be seen that a greater quantity of Mn_3O_4 increases the degradation efficiency. The excellent performance of the hybrid materials can therefore be reasonably attributed to of the functionalization with Mn_3O_4 which acts as a co-catalyst and lowers the charge recombination rate of the electron-hole pairs. The synergy of the two materials allows a faster production of oxidizing radicals which increases the degradation rate of MG in aqueous solution. The reaction rate was quantitatively assessed in terms of the change in MG concentration over time C_t with respect to its initial concentration C_o, as shown in Figure 12a. The curves show that the degradation of MG in aqueous solution depends on the time of illumination with UV light. The kinetics of the degradation of MG is first order for all hybrid photocatalysts Mn_3O_4@ZnO and the rate contants for samples 1, 2, 3 and 4 are calculated in 1.72×10^{-2} min, 2.38×10^{-2} min, 2.73×10^{-2} min, and 3.01×10^{-2} min, respectively, as shown in Figure 12b. The degradation efficiency for the four hybrid materials (samples 1, 2, 3 and 4) was calculatedas 93.22 %, 95.71 %, 96.67 %, and 97.40 % respectively, as shown in Figure 12c.

Overall, the degradation measurements of MB, MO and MG dyes demonstrated that Mn_3O_4@ZnO hybrid nanomaterials are excellent photocatalysts. The photocatalytic activity of the hybrid material with the maximum amount of Mn_3O_4 was the best for all three dytes, reaching almost 100%. For MG The performance of the various Mn_3O_4@ZnO hybrid materials for the degradation of MB, MO and MG is summarized in Table 1.

4. Conclusions

In this research work, we used sol gel and hydrothermal methods to synthesize different nanostructured materials basedon pristine ZnO and functionalized with different amounts of Mn_3O_4. The morphology turned out to be hierarchical composed of thin nanosheets, the composition containing only Zn, O and Mn and the structure composed of the hexagonal phases of ZnO and tetragonal of Mn_3O_4. The degradation performance of all tested dyes (MB, MO and MG) increased as the amount of Mn_3O_4 in the Mn_3O_4@ZnO hybrid photocatalyst increased. The material with the highest

amount of Mn_3O_4 (1 g) showed excellent degradation properties for all dyes: 94.59%, 89.99% and 97.40% for MB, MO and MG respectively. The degradation for all dyes followed first order kinetics. The rate constant values for the best catalyst were 8.51×10-3min for MB, 4.58×10^{-3}min for MO and 3.01×10^{-2} min for MG. The improved performance of hybrid materials can be attributed to the synergy between ZnO and Mn_3O_4 which leads to a high charge separation rate, a high density of catalytic sites and the generation of a large amount of oxidizing reactive species. These improvements suggest that Mn_3O_4 can be used as a dopant to increase the photocatalytic properties of other metal oxides such as TiO_2, SnO_2 and carbon-based materials.

Conflict of Interest

Authors declare no conflict of interest in this research study

4. References

[1]. K.A. Gusmao, L.V. Gurgel, T.M. Melo,L.F. Gil, J Environ Manag 2013,**118**,135–143.

[2]. K. Bhattacharya and A. Sharma, Kinetics and thermodynamics of methylene blue adsorption on neem (Azadirachta indica) leaf powder. Dyes Pigments 2005, **65**(1),51–59.

[3]. M. Anbia and S. Salehi, Removal of acid dyes from aqueous media by adsorption onto amino-functionalized nanoporous silica SBA-3. Dyes Pigments 2012, **94** (1), 1–9.

[4]. S. Nethaji, A. Sivasamy, G. Thennarasu and S. Saravanan, Adsorption of Malachite Green dye onto activated carbon derived from Borassus aethiopum flower biomass. J Hazard Mater 2010, **181** (1–3), 271–280.

[5]. A. M. Saad, M.R. Abukhadra, S.A.K. Ahmed, A.M. Elzanaty, A.H. Mady, M.A. Betiha, J.J. Shim and A.M. Rabie, Photocatalytic degradation of malachite green dye using chitosan supported ZnO and Ce–ZnO nano-flowers under visible light. J Environ Manage. 2020, **258**,110043.

[6]. A. Mohammadi, H. Daemi and M. Barikani, Fast removal of malachite green dye using novel superparamagnetic sodium alginate-coated Fe3O4 nanoparticles Int J Biol Macromol 2014, **69**,447–455

[7]. M. Jamshidi, M. Ghaedi, K. Dashtian, S. Hajati and A.A. Bazrafshan, Sonochemical assisted hydrothermal synthesis of ZnO: Cr nanoparticles loaded activated carbon for simultaneous ultrasound-assisted adsorption of ternary toxic organic dye: derivative spectrophotometric, optimization, kinetic and isotherm study.Ultrason Sonochem 2016, **32**,119–131

[8]. F.N. Azad, M. Ghaedi, K. Dashtian, S. Hajati and V. Pezeshkpour, Ultrasonically assisted hydrothermal synthesis of activated carbon–HKUST-1-MOF hybrid for efficient simultaneous ultrasound-assisted removal of ternary organic dyes and antibacterial investigation: Taguchi optimization. Ultrason Sonochem 2016, **31**,383–393

[9]. M.S. Chiou and G.S. Chuang, Competitive adsorption of dye metanil yellow and RB15 in acid solutions on chemically cross-linked chitosan beads. Chemosphere,2006, **62**,731–740

[10]. S. Sakthivel, B. Neppolian, M.V. Shankar, B. Arabindoo, M. Palanichamy and V. Murugesan, Solar photocatalytic degradation of azo dye: comparison of photocatalytic efficiency of ZnO and TiO2. Sol Energy Mater Sol Cells, 2003, **77**(1),65–82.

[11]. J.H. Sun, S.Y. Dong, J.L. Feng, X.J. Yin and X.C. Zhao, Enhanced sunlight photocatalytic performance of Sn-doped ZnO for Methylene Blue degradation. J Mol Catal A Chem, 2011, **335**,145–150.

[12]. L. Di, H. Yanga, T. Xian and X. Chen, Facile synthesis and enhanced visible-light photocatalytic activity of novel p-Ag3PO4/n-BiFeO3 heterojunction composites for dye degradation. Nanoscale Res Lett, 2018, **21**(5), 1–13.

[13]. Y. Zhou, H. Wenjihao, Yu. Jingang and F. Jiao, Effective photocatalytic degradation of methylene blue by Cu2O/MgAl layered double hydroxides. React Kinet Mech Catal 2015, **115**, 581–596.

[14]. Y. Haldorai and J.J. Shim, hitosan-zinc oxide hybrid composite for enhanced dye degradation and antibacterial activity. Composite Interfaces.2013 **20** (5), 365–377.

[15]. D. Pathania, D. Gupta, A.H. Al-Muhtaseb, G. Sharma, A. Kumar, M. Naushad, T. Ahamad and S.M. Alshehri, Photocatalytic degradation of highly toxic dyes using chitosan-g-poly (acrylamide)/ZnS in presence of solar irradiation. J Photochem Photobiol A Chem 2016, **329**, 61–68

[16]. A. Deng, J. Chen, H. Li, J. Ren, R. Sun, L. Zhao, Biol Res 2014, **9**(2), 2717–2726.

[17]. X. Liu, J. Zhang, L. Wang, T. Yang, X. Guo, S. Wu and S. Wang, 3D hierarchically porous ZnO structures and their functionalization by Au nanoparticles for gas sensors. J. Mater. Chem., 2011, **21**, 49-356.

[18]. Z.H. Jing and J.H. Zhan, Fabrication and gas-sensing properties of porous ZnO nanoplates. Adv. Mater., 2008, **20,** 4547-4551.

[19]. Y.C. Qiu, W. Chen and S.H. Yang, Facile hydrothermal preparation of hierarchically assembled, porous single-crystalline ZnO nanoplates and their application in dye-sensitized solar cells. J. Mater. Chem., 2010, **20,** 1001-1006.

[20]. D.C. Look, Recent advances in ZnO materials and devices Mater. Sci. Eng., B, 2001, **80,** 383-387.

[21]. X.J. Feng, L. Feng, M.H. Jin, J. Zhai, L. Jiang and D.B. Zhu, Reversible super-hydrophobicity to super-hydrophilicity transition of aligned ZnO nanorod films. J. Am. Chem. Soc., 2004, **126**, 62-63

[22]. L. Vayssieres, Growth of arrayed nanorods and nanowires of ZnO from aqueous solutions Adv. Mater., 2003, **15**, 464-466.

[23]. M.S. Arnold, P. Avouris, Z.W. Pan and Z.L. Wang, Field-effect transistors based on single semiconducting oxide nanobelts. J. Phys. Chem. B, 2003, **107**, 659-663

[24]. C.L. Kuo, T.J. Kuo and M.H. Huang, Hydrothermal synthesis of ZnO microspheres and hexagonal microrods with sheetlike and platelike nanostructures. J. Phys. Chem. B, 2005, **109,** 20115-20121.

[25]. X.W. Lou, Y. Wang, C. Yuan, J.Y. Lee and L.A. Archer, Template-free synthesis of SnO2 hollow nanostructures with high lithium storage capacity. Adv. Mater., 2006, **18,** 2325-2329.

[26]. X.W. Lou, C. Yuan and L.A. Archer, Shell-by-shell synthesis of tin oxide hollow colloids with nanoarchitectured walls: cavity size tuning and functionalization. Small, 2007, **3,** 261-265.

[27]. L. Robben, A.A. Ismail, S.J. Lohmeier, A. Feldhoff, D.W. Bahnemann and J.C. Buhl, Facile synthesis of highly ordered mesoporous and well crystalline TiO2: Impact of different gas atmosphere and calcination temperatures on structural properties. Chem. Mater., 2012, **24,** 1268-1275.

[28]. R.Q. Song, A.W. Xu, B. Deng, Q. Li and G.Y. Chen, From layered basic zinc acetate nanobelts to hierarchical zinc oxide nanostructures and porous zinc oxide nanobelts. Adv. Funct. Mater., 2007, **17,** 296-306.

[29]. B. Li and Y. Wang, Facile synthesis and enhanced photocatalytic performance of flower-like ZnO hierarchical microstructures. J. Phys. Chem. C, 2010, **114**, 890-896.

[30]. M. Osgouei, M. Saket, H. Khatamian and H. Kakili, Improved visible-light photocatalytic activity of Mn3O4-based nanocomposites in removal of methyl orange. Mater. Chem. Phys., 2020, **239**, 122108.

[31]. T. Shen, S. Xueke, G. Jiaxiu, L. Jing and Y. Shandong, Photocatalytic removal of NO by light-driven Mn3O4/BiOCl heterojunction photocatalyst: Optimization and mechanism. Chem. Eng. J., 2021, **408,** 128014.

[32]. Y. Ma, J. Jiang, A. Zhu, P. Tan, Y. Bian, W. Zeng, H. Cui and J. Pan, Enhanced visible-light photocatalytic degradation by Mn 3 O 4/CeO 2 heterojunction: a Z-scheme system photocatalyst. Inorg. Chem. Front., 2018, **5,** 2579-2586.

[33]. R. Rahimi, A. Mehrehjedy and S. Zargari, BiVO4/Mn3O4 a novel p–n heterojunction photocatalyst functionalized with metalloporphyrins: Synthesis, charge transfer mechanism, and enhanced visible-light photocatalysis for degradation of dye pollutant Environ. Prog. Sustain. Energy, 2017, **36** , 1439-1448.

[34]. Q. Ma, X. Zhang, R. Guo, H. Zhang, Q. Cheng, M. Xie and X. Cheng, Persulfate activation by magnetic γ-Fe2O3/Mn3O4 nanocomposites for degradation of organic pollutants. Separ. Purif. Technol., 2019, **210,** 335-342.

[35]. N. Li, Y. Tian, J. Zhao, J. Zhang, J. Zhang, W. Zuo and Y. Ding, Efficient removal of chromium from water by Mn3O4@ ZnO/Mn3O4 composite under simulated sunlight irradiation: synergy of photocatalytic reduction and adsorption. Appl. Catal., B, 2017, **214**, 126-136.

[36]. M.T. Qamar, M. Aslam, Z. Rehan, M.T. Soomro, J.M. Basahi, I.M. Ismail, T. Almeelbi and A. Hameed, The influence of p-type Mn3O4 nanostructures on the photocatalytic activity of ZnO for the removal of bromo and chlorophenol in natural sunlight exposure. Appl. Catal., B, 2017, **201,** 105-118

[37]. R. Saravanan, V.K. Gupta, V. Narayanan and A. Stephen, Visible light degradation of textile effluent using novel catalyst ZnO/γ-Mn2O3. J. Taiwan Inst. Chem. Eng., 2014, **45,** 1910-1917.

[38]. P.J. Shubha, H.S. Savitha, S.F. Adil, M. Khan, M.R. Hatshan, K. Kavalli and B. Shaik, Employing manufactured Mn3O4–ZnO nanocomposite for ameliorated photocatalytic performance under visible light. dyes Molecules, 2012, **26** (15), 4661.

[39]. S. Khan, A. Hussain, K. He, B. Liu, Z. Imran, J. Ambreen, S. Hassan, M. Ahmad, S. Sitwat Batool and C. Li, Tailoring the bandgap of Mn3O4 for visible light driven photocatalysis. J. Environ. Manag., 2021, **293**,112854.

[40]. M.T. Qamar, M. Aslam, Z. Rehan, M.T. Soomro, J.M. Basahi, I.M. Ismail, T. Almeelbi and A. Hameed, The influence of p-type Mn3O4 nanostructures on the photocatalytic activity of ZnO for the removal of bromo and chlorophenol in natural sunlight exposure. Appl. Catal., B, 2017, **201**, 105-118.

[41]. A.A. Ullah, A.F. Kibria, M. Akter, M.M.I. Khan, A.R.M. Tareq and S.H. Firoz, Oxidative degradation of methylene blue using Mn 3 O 4 nanoparticles. *Water Conservation Science and Engineering*, 2017, ***1***(4), 249-256.

[42]. N. Kumar, H. Mittal, L. Reddy, P. Nair, J.C. Ngila and V. Parashar, Morphogenesis of ZnO nanostructures: role of acetate (COOH−) and nitrate (NO 3−) ligand donors from zinc salt precursors in synthesis and morphology dependent photocatalytic properties. RSC Adv., 2015, **5**|, 38801-38809

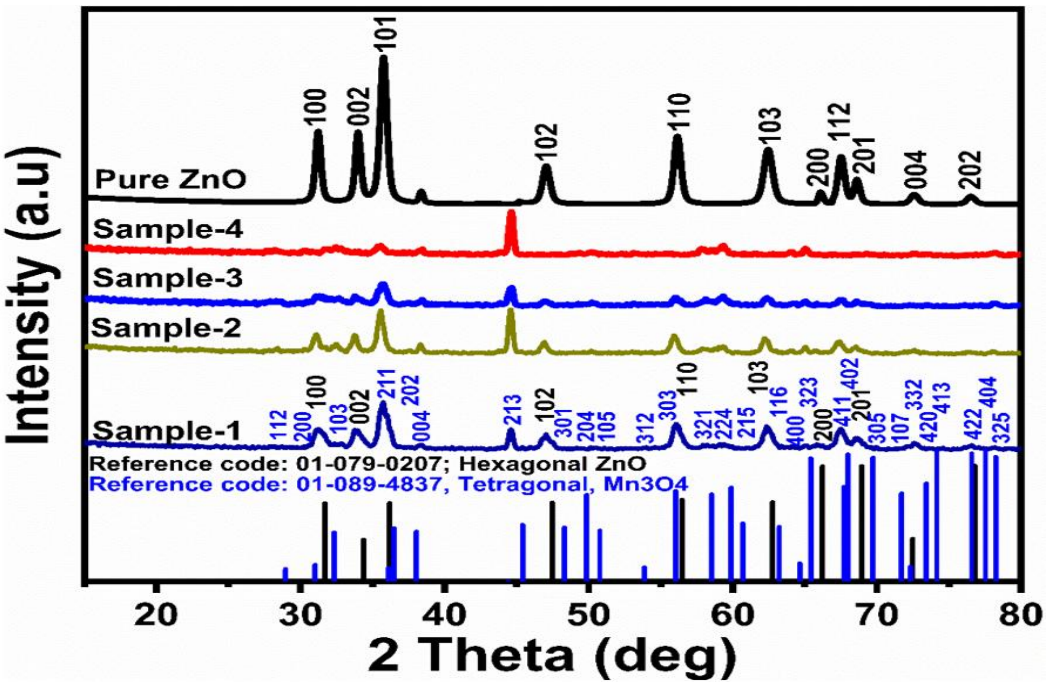

Figure1: (a) XRD patterns of pristine ZnO and ZnO doped with different amounts of Mn_3O_4 (b) shift comparison of the (220) peak for pristine ZnO and Mn_3O_4-doped samples.

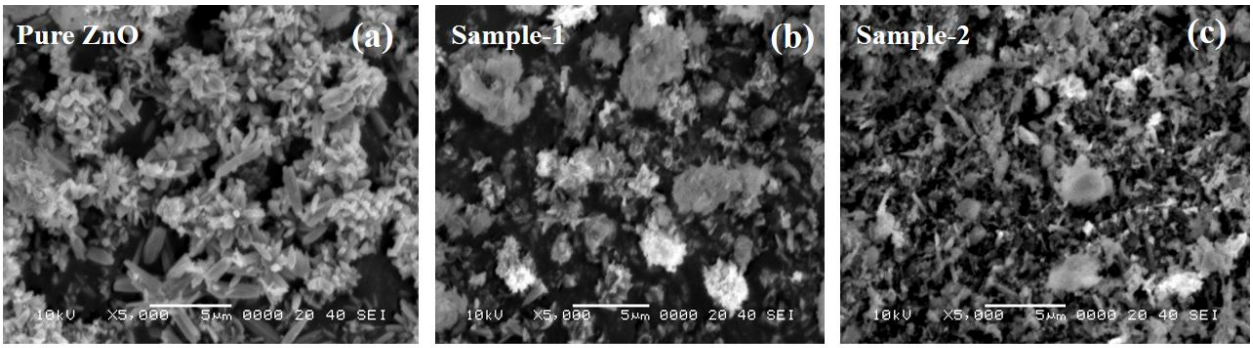

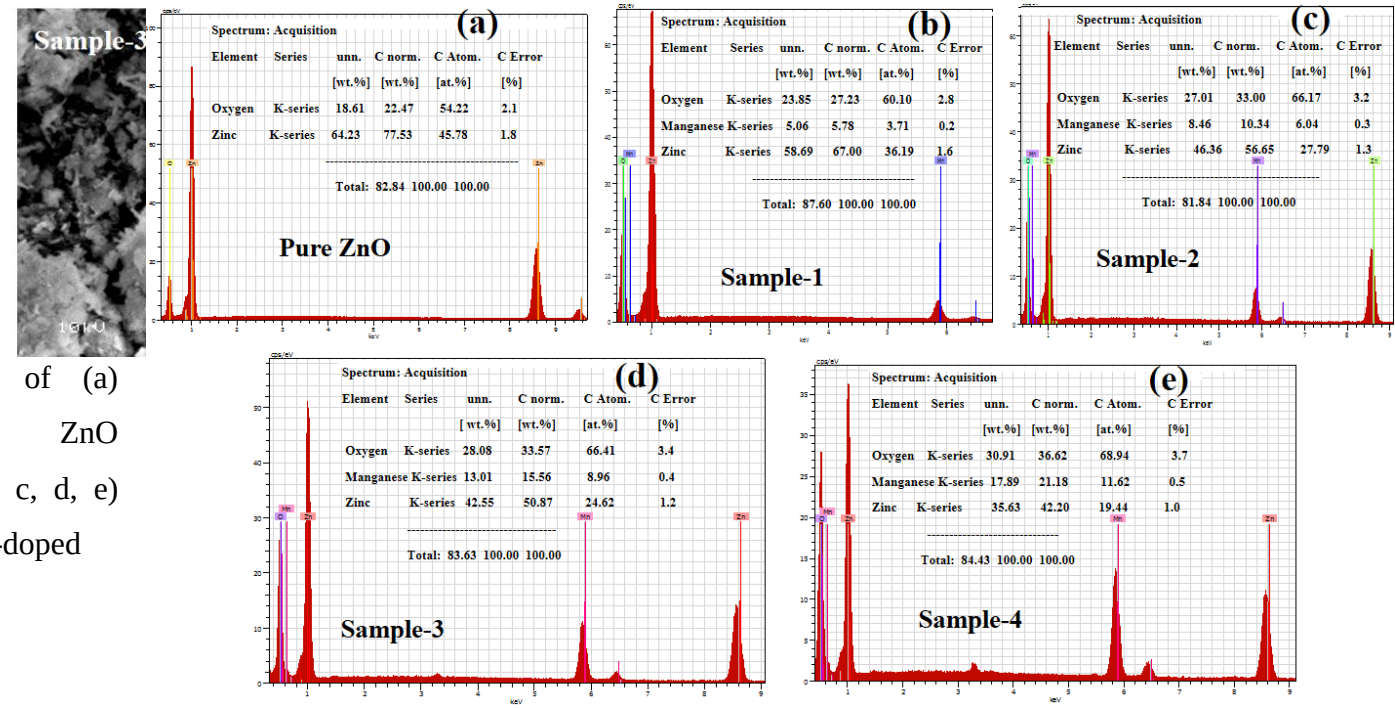

Figure 2: SEM images of (a) pristine ZnO and (b, c, d, e) Mn_3O_4-doped

ZnO materials synthesized

by sol-gel method

Figure 3: (a) EDX analysis of (a) pristine ZnO and (b, c, d, e) Mn_3O_4-doped ZnO material synthesized by Sol-gel method

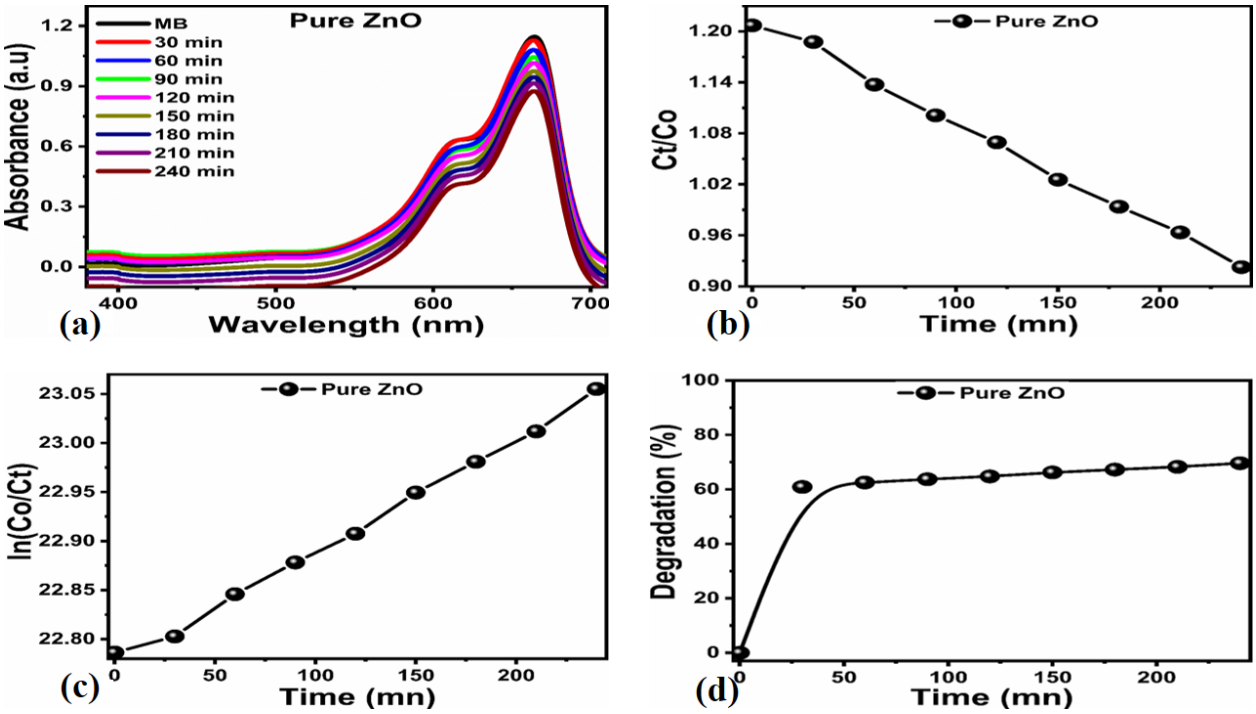

Figure 4: Degradation over time (240 min) of a solution of MB of concentration 1.87×10^{-5} M under irradiation with UV light in the presence of 5 mg of pristine ZnO. (a) UV-vis absorption spectra during dye degradation, (b) kinetics Ct/Co irradiation time, (c) LnCt/Co plot, (d) percent degradation of MB

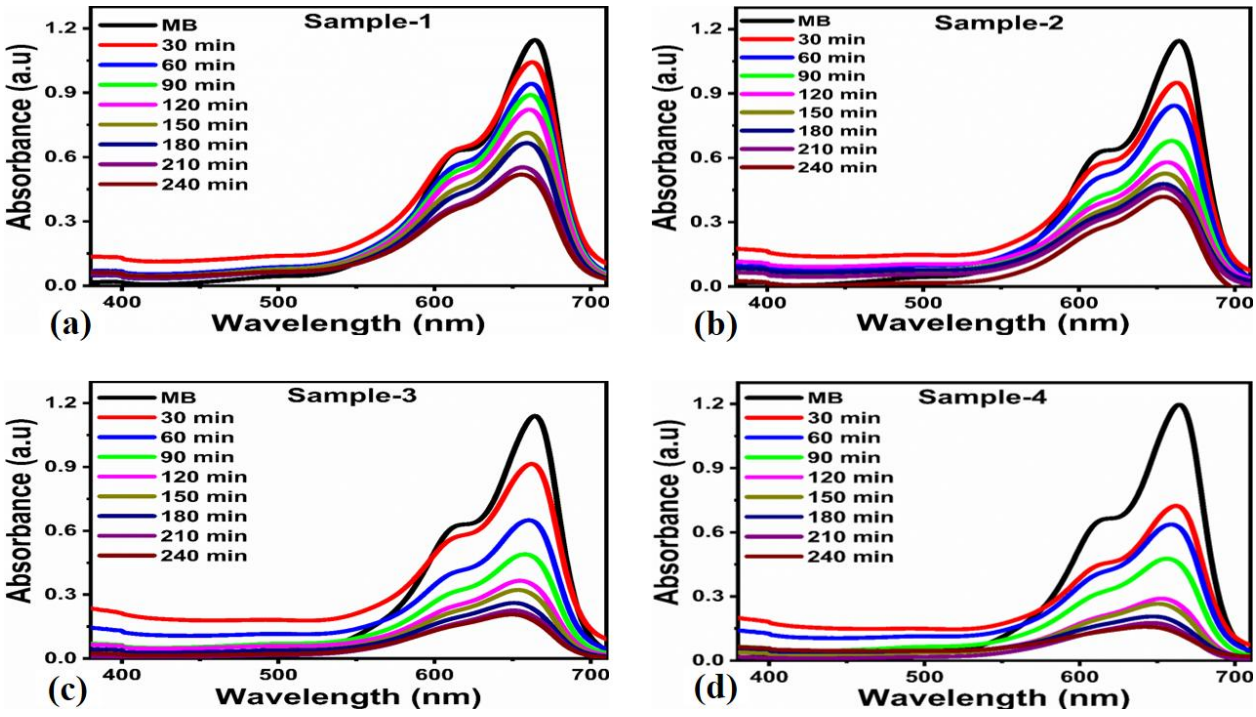

Figure 5: (a-d) UV-Vis absorption spectra of the MB solution at concen-

tration of 1.87×10^{-5}M using 5 mg photocatalyst dose of hybrid materials during photodegradation under UV light illumination using samples 1-4 as photocatalysts

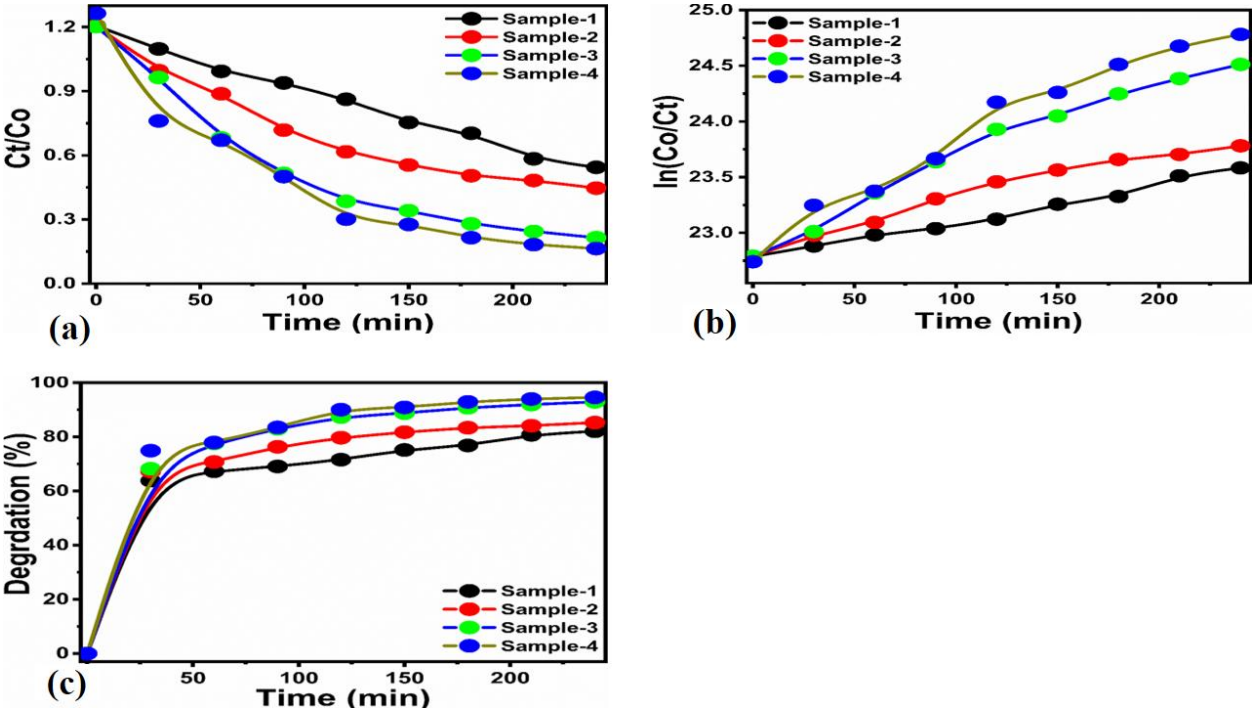

Figure 6: Degradation kinetics (a) kinetics Ct/Co irradiation time, (b) LnCt/Co plot, (c) percent degradation of MB

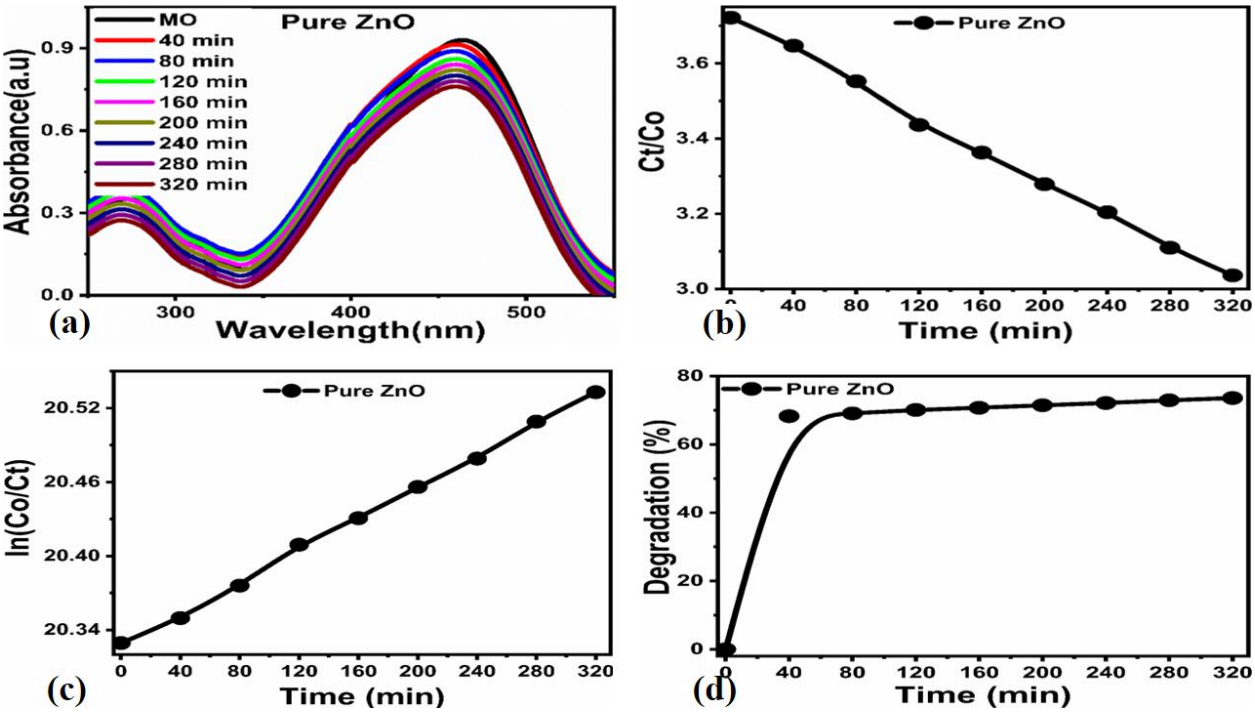

Figure 7: Degradation over time (320 min) of a solution of MO of concentration 2.44 × 10^{-5} M under irradiation with UV light in the presence of 5 mg of pristine ZnO. (a) Time

change of the UV-vis spectrum, (b) kinetics Ct/Co irradiation time, (c) LnCt/Co plot, (d) percent degradation of MO

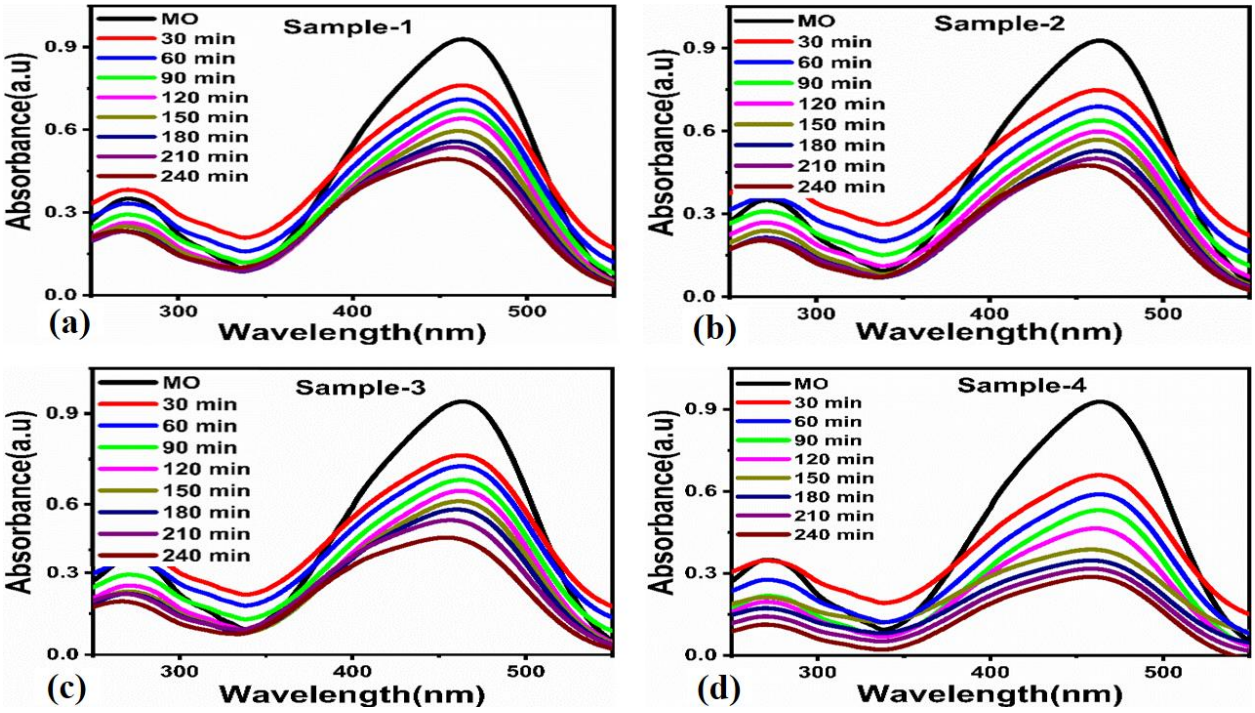

Figure 8: (a-d) UV-Vis absorption spectra MO solution at concentration of 2.44×10^{-5}M during photodegradation under UV light illumination using 5 mg dose of samples 1-4 as hybrid photocatalysts.

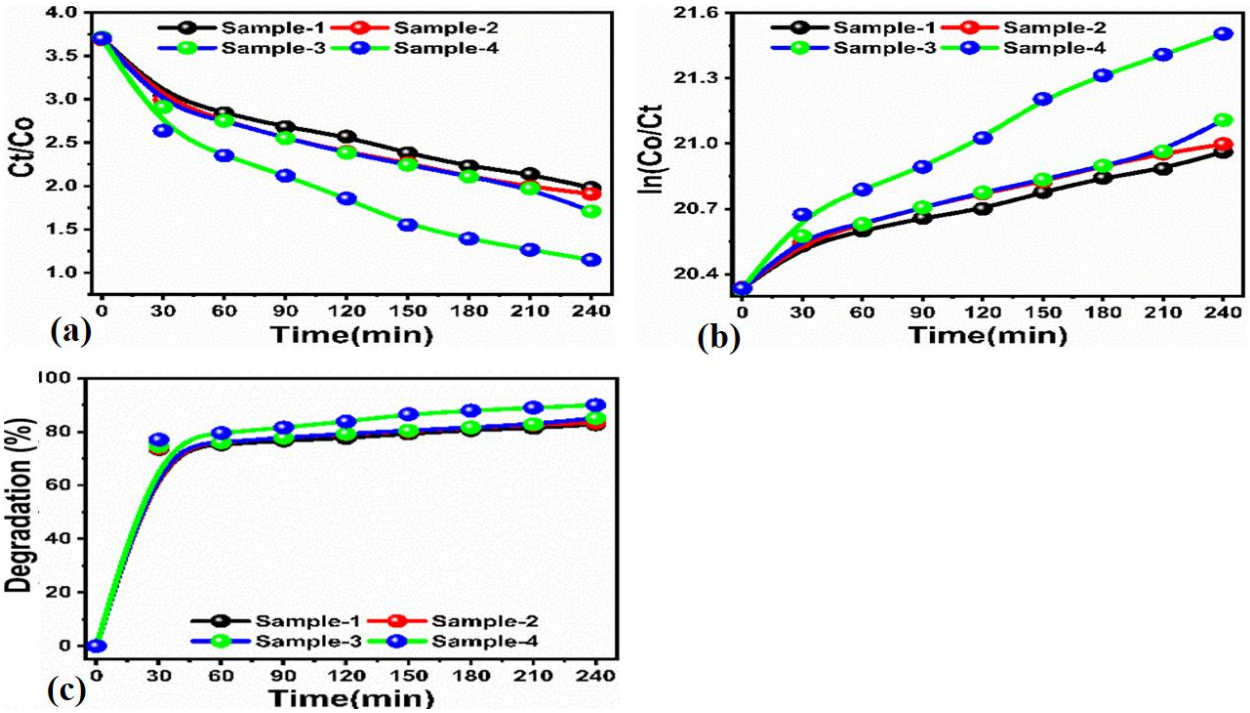

Figure 9: Degradation kinetics (a) kinetics Ct/Co irradiation time, (b) LnCt/Co plot, (c) percent degradation of MO

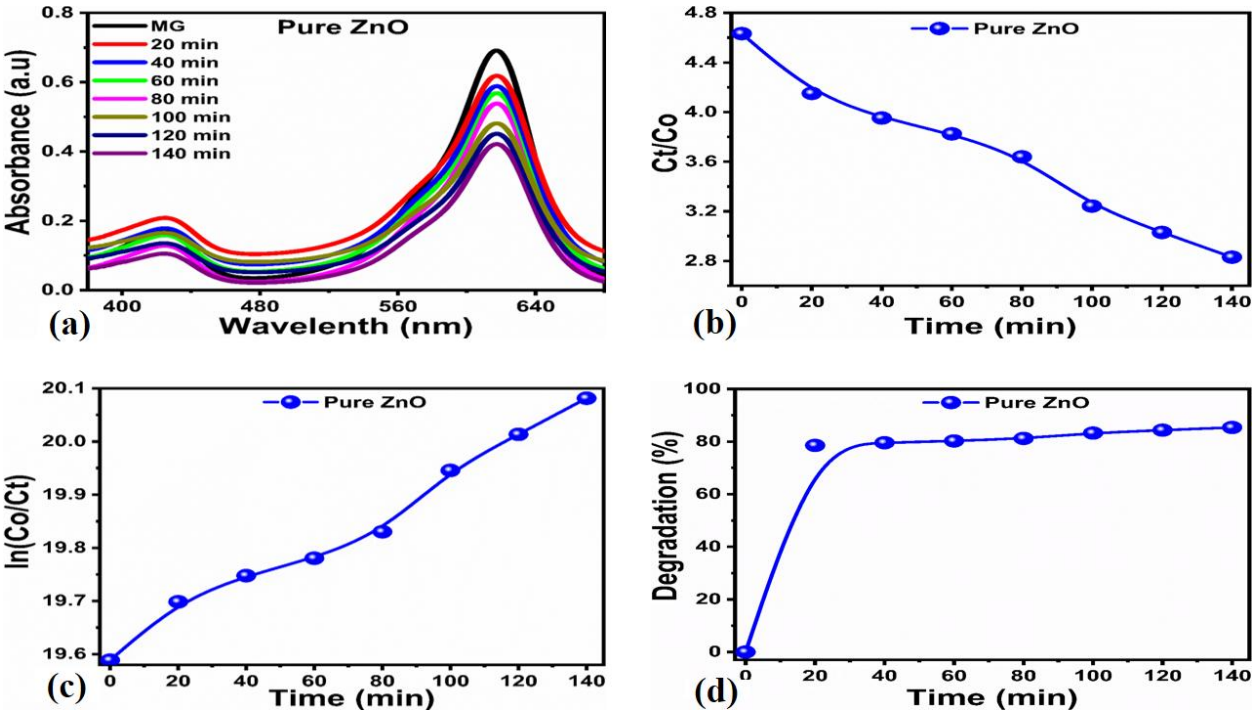

Figure 10: Degradation over time (140 min) of a solution of MG of concentration 5.48 × 10^{-5} M under irradiation with UV light in the presence of 5 mg of pristine ZnO. (a) Time change of the UV-vis spectrum, (b) Ct/Co over irradiation time, (b) kinetics Ct/Co irradiation time, (c) LnCt/Co plot, (d) percent degradation of MG

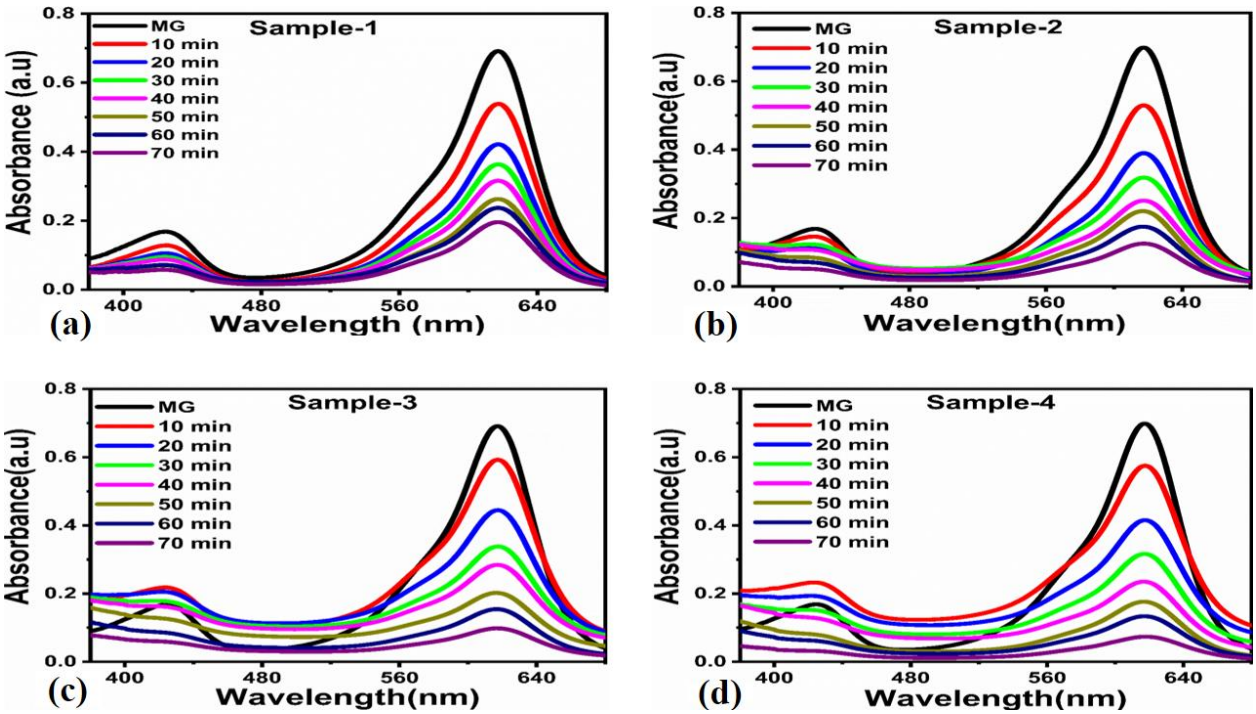

Figure 11: (a-d) change in the UV-Vis spectrum of the MG solution at concentration of 5.48×10^{-5}M during photodegradation under UV light irradiation using 5mg dose of samples 1-4 as photocatalysts.

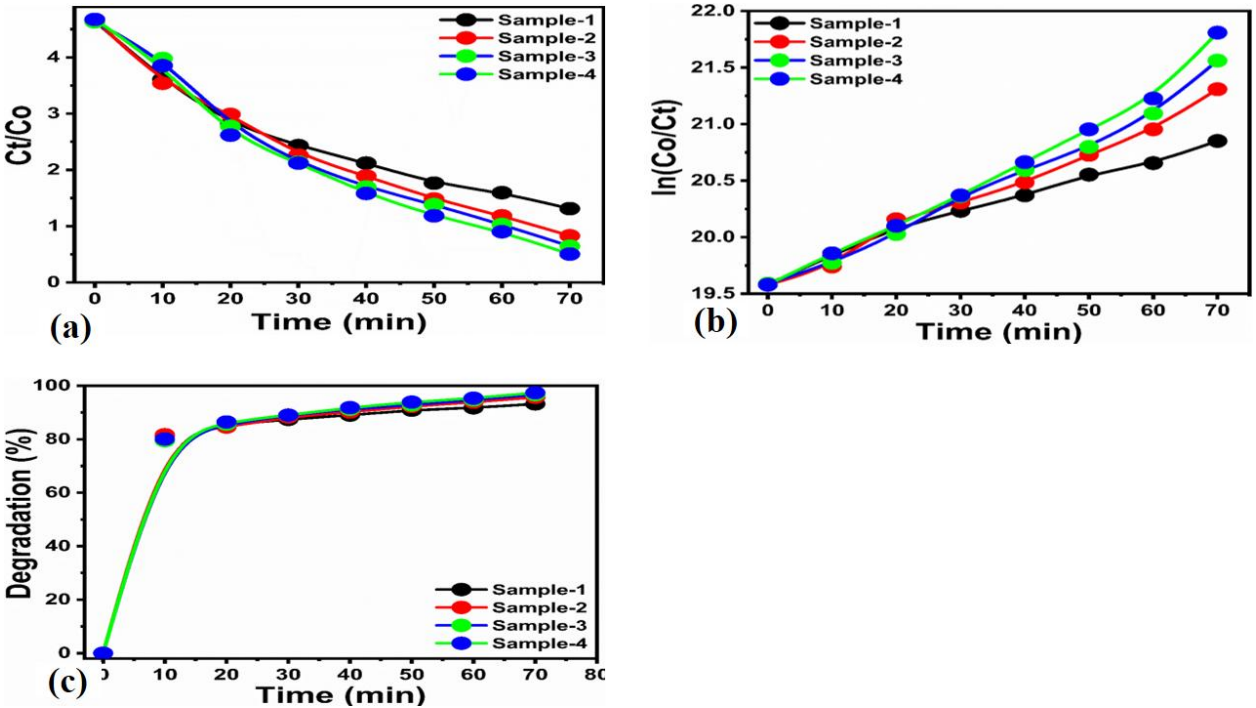

Figure 12: Degradation kinetics (a) kinetics Ct/Co

irradiation time, (b) LnCt/Co plot, (c) percent degradation of MG

Table 1: Summary of obtained results for the Photodegradation of various dyes using different Mn_3O_4@ZnO hybrid materials in comparison to pure ZnO.

Sample Name	Dye	Degradation %	Time (min)	Rate constant (K)
Pure ZnO	MB	69.60 %	240 min	1.14×10^{-3}min
	MO	73.56 %	320 min	6.43951E-4
	MG	85.37 %	140 min	3.37×10^{-3} min
Sample-1	MB	82.07 %	240 min	3.33×10^{-3}min
	MO	82.78 %	240 min	2.32×10^{-3}min
	MG	93.22 %	70 min	1.72×10^{-2} min
Sample-2	MB	85.28 %	240 min	4.19×10^{-3}min
	MO	83.38 %	240 min	2.50×10^{-3}min
	MG	95.71 %	70 min	2.38×10^{-2} min
Sample-3	MB	92.91 %	240 min	7.33×10^{-3}min
	MO	85.12 %	240 min	2.74×10^{-3}min
	MG	96.67 %	70 min	2.73×10^{-2} min
Sample-4	MB	94.59 %	240 min	8.51×10^{-3}min
	MO	89.99 %	240 min	4.58×10^{-3}min
	MG	97.40 %	70 min	3.01×10^{-2} min